Revisiting the Power Law Characteristics of the Plastic Shock Front under Shock Loading

Songlin Yao,[1] Jidong Yu,[1] Yinan Cui,[2,*] Xiaoyang Pei,[1] Yuying Yu,[1] and Qiang Wu[1,†]
[1]National Key Laboratory of Shock Wave and Detonation Physics, Institute of Fluid Physics, China Academy of Engineering Physics, Mianyang, Sichuan 621900, China
[2]Applied Mechanics Laboratory, School of Aerospace Engineering, Tsinghua University, Beijing 100084, China

(Received 31 December 2019; accepted 22 January 2021; published 26 February 2021)

Under uniaxial shock compression, the steepness of the plastic shock front usually exhibits power law characteristics with the Hugoniot pressure, also known as the "Swegle-Grady law." In this Letter, we show that the Swegle-Grady law can be described better by a third power law rather than the classical fourth power law at the strain rate between 10^5–10^7 s^{-1}. A simple dislocation-based continuum model is developed, which reproduced the third power law and revealed very good agreement with recent experiments of multiple types of metals quantitatively. New insights into this unusual macroscopic phenomenon are presented through quantifying the connection between the macroscopic mechanical response and the collective dynamics of dislocation assembles. It is found that the Swegle-Grady law results from the particular stress dependence of the plasticity behaviors, and that the difference between the third power scaling and the classical fourth power scaling results from different shock dissipative actions.

DOI: 10.1103/PhysRevLett.126.085503

Understanding the self-similar regularities of the dynamic response of solids under shock loading is the key for the development of universal methods for investigating the rheological properties and the destruction of condensed matter due to multiscale structural effects [1–7]. The "Swegle-Grady law" [8–10], describing the self-similarity of plastic wave fronts, is regarded as the most striking manifestations of the spatiotemporal dynamics [1,4], and continuous to receive considerable experimental [11–14] and theoretical attention [15–21] since it was proposed about 40 years ago [8,9]. However, the underlying mechanisms of this criticality are far from well understood until now. Previous studies [16,22] have demonstrated the important role of plasticity on the macroscopic power law. However, a clear quantitative understanding is still lacking. The complexity of this problem lies in that the shock compression process is so ultrafast [23–26], during which the elastic compression and the plastic relaxation is strongly coupled [27–28], while the present diagnostic techniques still cannot capture the evolution laws of the plasticity microstructures [23–26].

To understand this self-similarity, the well-known Grady's theoretical model [8] ignores the shock variance of the plastic dissipative action, and predicts the fourth power scaling between the strain rate and the Hugoniot pressure $\dot{\varepsilon} \sim p_h^4$. As the theoretical basis of the fourth power law, to the authors' knowledge, shock invariance of the dissipative action has never been verified rigorously. Mesoscopic experiments at 10^{10} s^{-1} published by Crowhurst *et al.* [13] tend to support this assumption and the fourth power scaling proposed by Grady for macroscopic experiments [29] at moderate strain rates. However, the divergence in the length scales of the tested samples and the strain rate ranges makes the conclusion suspicious. Particularly, the wave structure, from which the Swegle-Grady law is obtained, may vary with the propagating distance of shock wave [6]. In addition, the scaling exponent observed in some recent experiments [30–47] and that generated by multiscale simulations [15,18] are closer to 3 rather than 4 [see Figs. 4(a) and 4(b)]. Discrepancy between classical theory and recent experiments and simulations raises the suspicion of the fourth power law, and compels further research into the fundamental laws of this unusual phenomenon.

In this Letter, we avoid Grady's hypothesis on the shock invariance of the dissipative action, and demonstrate that the quantitative connection between the macroscopic power law and the dislocation behaviors can be derived theoretically. A dislocation-based continuum model is proposed from the perspective of energy. This model successfully reproduced the wave structures observed experimentally in multiple kinds of metals at the strain rate between 10^5–10^7 s^{-1}. This provides new insights that the essence of the macroscopic power law characteristic is the particular stress dependence of dislocation motion and generation.

Upon being subjected to a shock, materials are compressed to the Hugoniot state by the elastic precursor and the plastic shock wave together. The Hugoniot state is nearly a hydrostatic state, where the shear stress is much lower than the hydrostatic pressure [24,27,28]. This implies that the input shear strain energy by the shock is almost totally relaxed by the plastic dissipation. Considering that the stress increase in a macroscopic material induced by the elastic precursor is much lower than the Hugoniot pressure

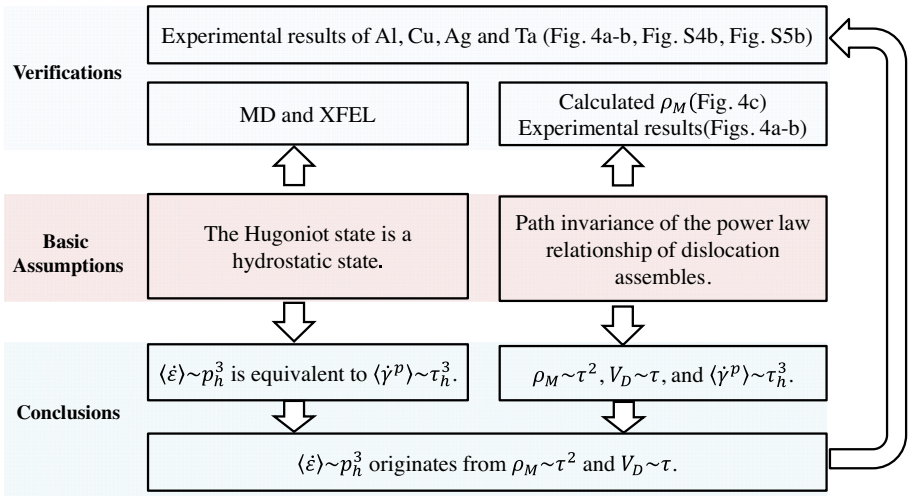

FIG. 1. Schematic plot showing the basic idea of our theoretical model. $\langle\dot{\varepsilon}\rangle$ is average strain rate, $\langle\dot{\gamma}^p\rangle$ is average plastic strain rate, p_h is Hugoniot pressure, τ is shear stress, τ_h is total input shear stress, ρ_M is dislocation density, and V_D is dislocation velocity. MD means molecular dynamics, XFEL means x-ray free electron laser.

due to the "elastic precursor decay" [6], and that the deformation on the elastic precursor is one-dimension elastic [6,24,28], the mechanical response on the elastic precursor can be neglected (see Sec. S3 [48]). Therefore, the energy conservation relation that the input shear strain energy is equal to the plastic dissipation energy on the plastic front is obtained. In the following, based on this relation, we are going to analyze the stress-strain relation on the plastic front with the aim to gain further insight into the power law characteristics of the plastic shock front. The basic idea of our theoretical model is schematically summarized in Fig. 1.

As schematically shown in Fig. 2, during the shock compression, the evolution of the resolved shear stress (RSS), the driving force for dislocation slip, can be written as

$$d\tau = 2m\mu(\dot{e}_{yy} - \dot{\gamma}_p)dt, \tag{1}$$

where e_{yy} is the longitudinal deviatoric strain $e_{yy} = \frac{2}{3}\varepsilon$, y denotes the loading direction, ε is the longitudinal strain, γ_p is the plastic strain, a superposed dot means a time derivative, μ is the shear modulus, and m is the projection factor. The linear elasticity relation in Eq. (1) to describe the shear deformation is reasonable because the elastic deviatoric strain on the plastic front is very small (see Sec. S4 [48]).

Inspired by Grady [10], we use the "fastest rising portion" (see S10 and Fig. S7 [48]) of the plastic front to replace the plastic front when performing the analysis. On the plastic front, the increase and decrease of RSS due to the shock compression and plastic relaxation can be written as

$$\tau_h - \tau_0 = \int_{t_0}^{t_1} 2m\mu\dot{e}_{yy}dt, \tag{2}$$

$$\tau_h - \tau_C = \int_{t_0}^{t_1} 2m\mu\dot{\gamma}_p dt, \tag{3}$$

where t_0 and t_1 are the beginning time and the ending time of the plastic front, τ_0 is the RSS at the Hugoniot elastic limit (HEL), τ_c is the critical resolved shear stress (CRSS) at the Hugoniot state, and $\tau_h = 2m\mu e_h$ is defined as the total input shear stress by the shock compression with plastic relaxation neglected (see Fig. 2 and Sec. S5 [48]). $e_h = \frac{2}{3}(u_h/D)$ is the longitudinal deviatoric strain at the Hugoniot state, where u_h is the particle velocity at Hugoniot state, $D = C_0 + su_h$ is the shock velocity, s and C_0 are the parameters of shock Hugoniot relation. If $u_h \ll D$, which holds well in this work, D is approximately equal to C_0. Thus, τ_h is proportional to p_h, $p_h = \rho_0 D u_h$ (see Sec. S12 [48]).

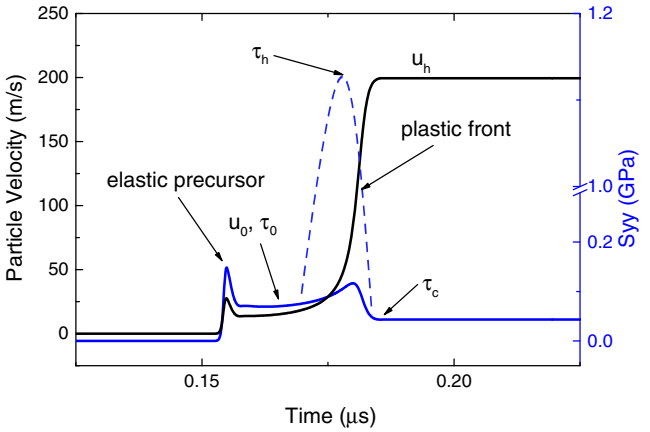

FIG. 2. Calculated time histories of particle velocity and longitudinal deviatoric stress. Blue solid line denotes the deviatoric stress along the real path, blue dashed line denotes the deviatoric stress along the virtual path, and black solid line denotes the particle velocity.

As mentioned above, τ_0 is much lower than p_h due to the elastic precursor decay. The hydrostatic state at the Hugoniot state implies that τ_c is also much lower than p_h. Given that τ_h is comparable to p_h, the right-hand side of Eq. (2) is approximately equal to that of Eq. (3),

$$\int_{t_0}^{t_h} 2m\mu\dot{e}_{yy}dt = \int_{t_0}^{t_1} 2m\mu\dot{\gamma}_p dt. \tag{4}$$

If both sides of Eq. (4) are divided by the rise time, $\Delta t_{\text{rise}} = t_1 - t_0$, the conclusion is gained that the average strain rate, $\langle\dot{\varepsilon}\rangle = (1/\Delta t_{\text{rise}})\int_{t_0}^{t_1}\dot{\varepsilon}dt$, is linear to the average plastic strain rate, $\langle\dot{\gamma}_p\rangle = (1/\Delta t_{\text{rise}})\int_{t_0}^{t_1}\dot{\gamma}_p dt$. This is consistent with Molinari *et al.*'s derivation based on continuum mechanics [16]. Thus the power scaling relationship of $\dot{\varepsilon}$ with p_h, $\langle\dot{\varepsilon}\rangle \sim p_h^n$, where n is the scaling coefficient, is equivalent to the power scaling relationship of $\dot{\gamma}_p$ with τ_h, $\langle\dot{\gamma}_p\rangle \sim \tau_h^n$. Therefore, in the following, we aim to address the power scaling relationship from the viewpoint of plastic relaxation.

A thermoelastic-viscoplastic model is used to address this behavior. The details of this model can be found in our previous work [56]. The essence of the viscoplastic model is the governing equation of the dislocation multiplication rate proposed from that a fixed portion of the dissipated energy, about 10% [57] and controlled by the multiplication coefficient, provides the energy needed for newly generated dislocations. The governing equation is expressed as

$$(d\rho_M/dt) = \alpha_{\text{mult}}(\tau\dot{\gamma}_p/\mu b^2), \tag{5}$$

where $\tau\dot{\gamma}_p$ is the dissipation rate of plastic strain energy density, α_{mult} is the multiplication coefficient and depends on materials, b is the burgers vector, and μb^2 is linear to the elastic energy per unit length of dislocation. α_{mult} as well as other model parameters are listed in Table S2 [48].

Using this model, we successfully reproduce the wave structures and the power law scaling of multiple kinds of metals, including aluminum, copper, silver, and tantalum. The plate-impact experiments are simulated at different applied stresses. Simulated wave profiles of aluminum and copper, as shown in Figs. 3(a) and 3(b), and those of other metals (see Figs. S4 and S5 [48]) match remarkably well with experimental results on the critical features, including the HEL and the plastic front. The calculated dislocation density at the Hugoniot state is in general agreement with experimentally observed residual dislocation density in recovered aluminum and that predicted by Austin's model [18] and dislocation dynamics (DD) simulations [58] [see Fig. 4(c)].

Model-predicted power law characteristics of the strain rate with the Hugoniot pressure also match well with recent experiments [30–47] at the strain rate between 10^5 and 10^7 s^{-1} [see Figs. 4(a) and 4(b)]. In particular, the fitted scaling coefficient of aluminum is ~3.0, close to 3.3

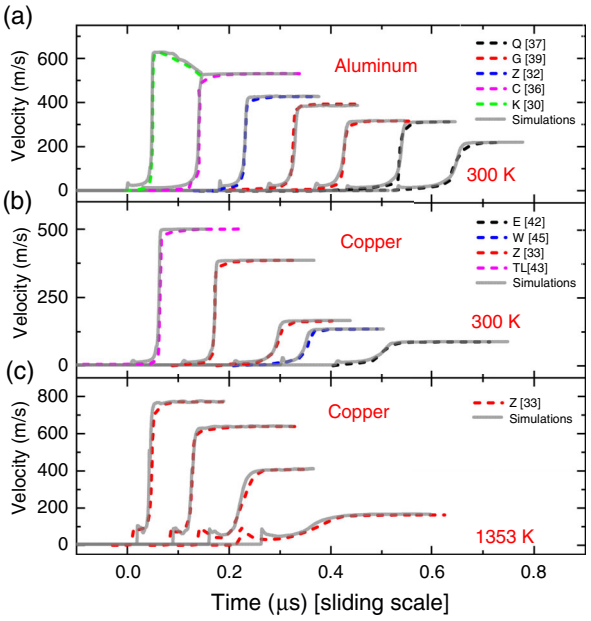

FIG. 3. Comparison of calculated velocity profiles with experimental results: (a) aluminum at 300 K; (b) copper at 300 K; (c) copper at 1353 K.

proposed by Holian *et al.* [15] and Austin *et al.* [18], while that of copper is about 2.32. We did not address the strain rate-stress relation obtained from mesoscopic experiments at the strain rate of ~10^{10} s^{-1} because the deformation mechanisms at such extreme conditions are still poorly understood, which may be beyond the capability of the

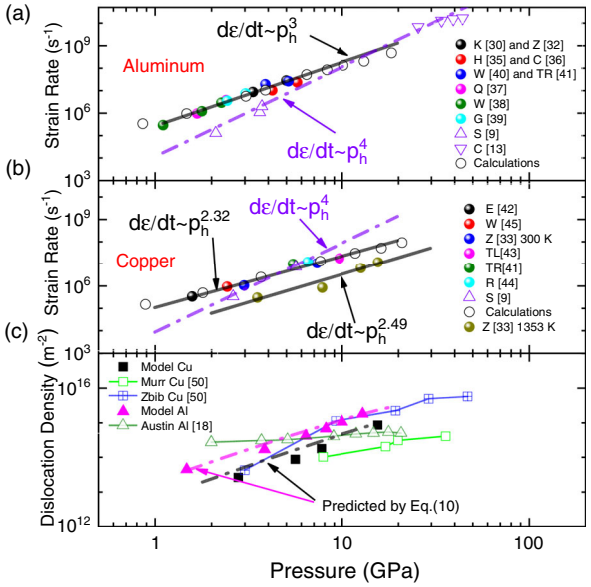

FIG. 4. Comparison of calculated results and experiments: (a) aluminum; (b) copper; c) dislocation density. The violet dash dotted lines in (a) and (b) is the fourth power relation, while the dash dotted lines in (c) denote the dislocation densities of aluminum and copper predicted by Eq. (10).

current model. Apart from aluminum and copper, our model-predicted scaling coefficients of silver and tantalum at the same strain rate range, which are 2.5 and 3.1, respectively, are also in good agreement with experimental results of silver [31] and tantalum [34,46,47] (see Figs. S4 and S5 [48]).

To further elucidate the power law scaling behavior and the dependence of scaling exponent on the materials, a virtual path for the evolution of the RSS is established based on energy conservation, along which the RSS is firstly compressed to τ_h by purely elastic deformation and subsequently relaxed to τ_c by purely plastic deformation, as shown in Fig. 2. The establishment of the virtual path is to simplify the analysis of the dislocation density because it is hard to obtain the analytical expression of the dislocation density along the real path (see Sec. S5 [48]). This path guarantees that the input shear strain energy and the dissipated shear strain energy are the same as those along the real path, which is justified in the following.

Along the real path, the shear strain energy at the Hugoniot state can be written as

$$E^h_{\mathrm{shr}} = \int_0^{e_{yy}} 2\mu(e-\gamma_p)de, \tag{6}$$

where e is the deviatoric strain, and γ_p is the plastic strain. For simplification, we use the longitudinal component of the shear strain energy to represent the shear strain energy. The first term of Eq. (6) is the input shear strain energy, $E_{\mathrm{shr}} = \int_0^{e_{yy}} 2\mu e de = \mu e_{yy}^2$, while the second term is the plastically dissipated energy, $E_{\mathrm{dissip}} = \int_0^{e_{yy}} 2\mu\gamma_p de$. As mentioned above, the shear stress at the Hugoniot state is almost negligible. Thus E^h_{shr} can be neglected, and E_{shr} is approximately equal to E_{dissip}. Along the virtual path, the input shear strain energy, $E^v_{\mathrm{shr}} = \int_0^{e_{yy}} 2\mu e de = \mu e_{yy}^2$, equals to E_{shr}, and the dissipated energy, $E^v_{\mathrm{dissip}} = E^v_{\mathrm{shr}}$, equals to E_{dissip}.

If the dissipated energies along two paths are the same, the densities of newly generated dislocations along two paths are also the same provided that a fixed portion of the dissipated energy provides the energy needed for newly generated dislocations [57], which can be guaranteed by our constitutive model. Thus, we can perform theoretical analysis on the dislocation density with our model along the virtual path to gain an insight into the dislocation density evolution along the real path.

Along the virtual path, the elastic deformation and the plastic deformation are decoupled. Thus, the shear stress-plastic strain rate relationship can be expressed as

$$d\tau = -2m\mu\dot{\gamma}_p dt. \tag{7}$$

The time integral of the dislocation density can be replaced by a stress integral based on Eq. (7). Substituting Eq. (7) into Eq. (5), the relationship between dislocation density and the RSS can be written as

$$d\rho_M = -\frac{\alpha_{\mathrm{mult}}\tau d\tau}{2m\mu^2 b^2}. \tag{8}$$

To a good approximation, we neglected the evolution of other dislocation substructures when integrating the dislocation density governing equation because the evolution rates of other dislocation substructures are at least one order of magnitude lower than the multiplication rate on the plastic shock front (see Fig. S3 [48]). Integrating Eq. (8) with respect to the RSS from τ to τ_C along the plastic part of the virtual path, dislocation density can be expressed as

$$\rho_M(\tau) \approx \rho_0 + \frac{\alpha_{\mathrm{mult}}(\tau^2-\tau_C^2)}{4m\mu^2 b^2}. \tag{9}$$

If the upper limit of the integration is set as τ_h, the dislocation density is

$$\rho_M(\tau_h) \approx \frac{\alpha_{\mathrm{mult}}\tau_h^2}{4m\mu^2 b^2}, \tag{10}$$

considering that ρ_0 is much smaller than $\rho_M(\tau_h)$ and τ_C is much smaller than τ_h. Equation (10) implies that the scaling coefficient of dislocation density with p_h is 2 given that τ_h is linear to p_h. From Eq. (10), we can infer that the dislocation density along the real path also exhibits quadratic stress dependence. The quadratic stress dependent dislocation densities predicted by Eq. (10) of aluminum and copper are in good agreement with model-predicted results along the real path, as shown in Fig. 4(c), which indicates that it is reasonable to analyze the evolution of dislocation density with the aid of the virtual path, and that the constitutive model and the theoretical analysis along the virtual path are consistent. Moreover, the predicted scaling coefficient of the dislocation density with p_h is comparable to 1.7 obtained by DD simulations [58].

Following the same procedure, we can also obtain the stress dependence of dislocation density if other dislocation density equations are employed. For example, the scaling coefficient obtained from the equation used by Devincre *et al.* [59] is 2, while that by Wang *et al.* [60] is 1.43 (see Sec. S6 [48]). Both are comparable to the theoretical prediction of this article.

With respect to the dislocation velocity, its dependence on shear stress can be expressed as

$$V_D = A_0\tau^\alpha, \tag{11}$$

where A_0 is a constant and α describes the stress sensitivity of V_D, as discussed later.

Combining Eqs. (9) and (11), one can obtain the stress dependence of the plastic strain rate, $\dot{\gamma}^p = \{[A_0\alpha_{\mathrm{mult}}\tau^\alpha(\tau^2-\tau_C^2)]/[4m\mu^2 b]\}$. The power law characteristic of the average plastic strain rate can be estimated by

integrating the plastic strain rate with respect to τ along the virtual path,

$$\langle \dot{\gamma}_p \rangle = \frac{1}{\tau_C - \tau_h} \int_{\tau_h}^{\tau_C} \dot{\gamma}^p(\tau) d\tau \approx \eta \tau_h^\beta, \tag{12}$$

where η is a constant, the scaling coefficient $\beta = 2 + \alpha$ and τ_C is neglected because it is much lower than τ_h. Below the CRSS, the thermal activation dominates, $\alpha > 1$ [2,61], and $\beta > 3$, which may explain the transition of rate sensitivity of the flow stress at the strain rate around 10^3–10^4 s^{-1} [such as Fig. 3(b) in [62]]. Given that the shock induced shear stress surpasses the CRSS of the metals of interest quickly, phonon drag and the relativistic effect dominate dislocation motion for the considered strain rate range. If phonon drag dominates, $\alpha = 1$ [2,63], and $\langle \dot{\gamma}_p \rangle$ is cubic shear stress dependence, $\langle \dot{\gamma}_p \rangle \sim (\tau_h)^3$. If V_D approaches the transverse sound speed, relativistic effect dominates, α decreases toward 0 [2,63], and β gradually drops from 3 to 2 as applied stress increases, which can explain why the scaling coefficient of copper and silver, whose transverse sound speeds are easier to be achieved than aluminum, is closer to 2 than 3. The scaling coefficients predicted by Eq. (12) match well with model-predicted results and experimental results [see Figs. 4(a) and 4(b)]. Here, the average plastic strain rate along the virtual path is overestimated because the maximum RSS along the real path is much lower than τ_h due to the strong coupling between the shock compression and the plastic relaxation along the real path, as shown in Fig. 2. Nonetheless, the power law characteristics of the plastic strain rate along two paths are the same because the stress dependence of the dislocation velocity and that of the dislocation density are path invariance.

Then, why does our model deviate from the previous proposed fourth power law? When deriving it, Grady assumed that the dissipative action keeps invariant with the strain rate [8–10,64]. As opposed to Grady's hypothesis, the key hypothesis of our explanation of the third power law is that the plastic dissipation energy is related to the dislocation generation rate. Our calculated results suggest that the dissipative action exhibits power law scaling with the strain rate. The calculated scaling coefficient of the dissipative action with the strain rate of aluminum is ~0.36 at the strain rate between 10^5 and 10^7 s^{-1} (see Fig. S8 [48]). The dissipative action is written as, $A = \theta \dot{\varepsilon}^{0.36}$, where θ is a constant. When deriving the fourth power law, the following expression is obtained by Grady with the hypothesis that A is a constant, $\dot{\varepsilon} = [S/3A\rho_0(\rho_0 C_0^2)^3] p_h^4$. If one substitutes the strain rate dependent A into Grady's theoretical model, the scaling coefficient becomes 2.94, in accordance with our model-predicted scaling coefficient. Therefore, different conclusions of our work and Grady's work result from different dissipative actions.

A conclusion can be gained that the power law characteristics of the plastic shock front is determined by the stress dependence of the plastic behaviors. In particular, the linear stress dependence of dislocation velocity and the quadratic stress dependence of dislocation density contribute to the third power law together. In this sense, it is expected that the relationship of the strain rate with the Hugoniot pressure at other conditions, e.g., at elevated temperature, will also exhibit third power law as long as the evolution laws of dislocations keep the same. Experimental results and calculated results, generated by the same model, at elevated temperature validated this expectation to some extent, as shown in Figs. 3(c) and 4(b).

This work was supported by Science Challenge Project (Grant No. TZ2018001), the National Natural Science Foundation of China (Grants No. 11532012, No. 11702277, and No. 11972208), and the Foundation of National Key Laboratory of Shock Wave and Detonation Physics (Grant No. 6142A03191001).

*Corresponding author.
cyn@mail.tsinghua.edu.cn
†Corresponding author.
wuqianglsd@163.com

[1] Y. Bayandin, N. Saveleva, and O. Naimark, Frattura ed Integrità Strutturale, **49**, 243 (2019).
[2] M. Meyers, *Dynamic Behavior of Materials* (John Wiley, New York, 1994).
[3] M. A. Meyers, H. Jarmakani, E. M. Bringa, and B. A. Remington, in *Dislocations in Solids*, edited by J. P. Hirth and L. Kubin (North-Holland, The Netherlands, 2009), Vol. 15, pp. 91–197.
[4] D. J. Funk *et al.*, A summary report on the 21st century need and challenges of compression science workshop, Los Alamos National Laboratory Report, LA-UR-09-07771, 2009.
[5] J. Yu, W. Wang, and Q. Wu, Phys. Rev. Lett. **109**, 115701 (2012).
[6] B. Gurrutxaga-Lerma, D. S. Balint, D. Dini, D. E. Eakins, and A. P. Sutton, Phys. Rev. Lett. **114**, 174301 (2015).
[7] Y. Cui, G. Po, Y.-P. Pellegrini, M. Lazar, and N. Ghoniem, J. Mech. Phys. Solids **126**, 20 (2019).
[8] D. E. Grady, Appl. Phys. Lett. **38**, 825 (1981).
[9] J. W. Swegle and D. E. Grady, J. Appl. Phys. **58**, 692 (1985).
[10] D. E. Grady, J. Appl. Phys. **107**, 013506 (2010).
[11] M. A. Meyers, F. Gregori, B. K. Kad, M. S. Schneider, D. H. Kalantar, B. A. Remington, G. Ravichandran, T. Boehly, and J. S. Wark, Acta Mater. **51**, 1211 (2003).
[12] J. A. Hawreliak *et al.*, Phys. Rev. B **83**, 144114 (2011).
[13] J. C. Crowhurst, M. R. Armstrong, K. B. Knight, J. M. Zaug, and E. M. Behymer, Phys. Rev. Lett. **107**, 144302 (2011).
[14] A. J. Comley, B. R. Maddox, R. E. Rudd, S. T. Prisbrey, J. A. Hawreliak, D. A. Orlikowski *et al.*, Phys. Rev. Lett. **110**, 115501 (2013).
[15] B. L. Holian and P. S. Lomdahl, Science **280**, 2085 (1998).

[16] A. Molinari and G. Ravichandran, J. Appl. Phys. **95**, 1718 (2004).
[17] A. Molinari and G. Ravichandran, J. Mech. Phys. Solids **54**, 2495 (2006).
[18] R. A. Austin and D. L. McDowell, Int. J. Plast. **27**, 1 (2011).
[19] G. A. Malygin, S. L. Ogarkov, and A. V. Andriyash, Phys. Solid State **55**, 780 (2013).
[20] M. Kattoura and M. A. Shehadeh, Philos. Mag. Lett. **94**, 415 (2014).
[21] M. A. Shehadeh and H. M. Zbib, Philos. Mag. **96**, 2752 (2016).
[22] J. N. Johnson and L. M. Barker, J. Appl. Phys. **40**, 4321 (1969).
[23] M. J. Suggit, A. Higginbotham, J. A. Hawreliak, G. Mogni, G. Kimminau, P. Dunne, A. J. Comley, N. Park, B. A. Remington, and J. S. Wark, Nat. Commun. **3**, 1224 (2012).
[24] D. Milathianaki, S. Boutet, G. J. Williams, A. Higginbotham, D. Ratner, A. E. Gleason *et al.*, Science **342**, 220 (2013).
[25] M. Sliwa, D. McGonegle, C. Wehrenberg, C. A. Bolme, P. G. Heighway, A. Higginbotham *et al.*, Phys. Rev. Lett. **120**, 265502 (2018).
[26] S. J. Turneaure, P. Renganathan, J. M. Winey, and Y. M. Gupta, Phys. Rev. Lett. **120**, 265503 (2018).
[27] E. M. Bringa, A. Car, Y. Wang, M. Victoria, J. M. McNaney, B. A. Remington *et al.*, Science **309**, 1838 (2005).
[28] E. M. Bringa, K. Rosolankova, R. E. Rudd, B. A. Remington, J. S. Wark, M. Duchaineau, D. H. Kalantar, J. Hawreliak, and J. Belak, Nat. Mater. **5**, 805 (2006).
[29] L. B. Barker, *Behavior of Dense Media under High Dynamic Pressures* (Gordon and Breach, New York, 1968), p. 483.
[30] G. I. Kanel, S. V. Razorenov, K. Baumung, and J. Singer, J. Appl. Phys. **90**, 136 (2001).
[31] E. B. Zaretsky and G. I. Kanel, J. Appl. Phys. **110**, 073502 (2011).
[32] E. B. Zaretsky and G. I. Kanel, J. Appl. Phys. **112**, 073504 (2012).
[33] E. B. Zaretsky and G. I. Kanel, J. Appl. Phys. **114**, 083511 (2013).
[34] E. B. Zaretsky and G. I. Kanel, J. Appl. Phys. **115**, 243502 (2014).
[35] H. Huang and J. R. Asay, J. Appl. Phys. **100**, 043514 (2006).
[36] X. Chen, J. R. Asay, S. K. Dwivedi, and D. P. Field, J. Appl. Phys. **99**, 023528 (2006).
[37] M. Qi, H. He, and S. Yan, Chin. Phys. Lett. **24**, 8 (2007).
[38] Y. Wang, M. Qi, H. He, and L. Wang, Mech. Mater. **69**, 270 (2014).
[39] B. Glam, D. Moreno, S. Eliezer, and D. Eliezer, AIP Conf. Proc. **1426**, 987 (2012).
[40] J. M. Winey, B. M. Lalone, P. B. Trivedi, and Y. M. Gupta, J. Appl. Phys. **106**, 073508 (2009).
[41] S. J. Turneaure and Y. M. Gupta, J. Appl. Phys. **106**, 033513 (2009).
[42] J. P. Escobedo, E. K. Cerreta, D. Dennis-Koller, B. M. Patterson, and C. A. Bronkhorst, J. Phys. Conf. Ser. **500**, 112023 (2014).
[43] W. D. Turley, S. J. Fensin, R. S. Hixson, D. R. Jones, B. M. La Lone, G. D. Stevens, S. A. Thomas, and L. R. Veeser, J. Appl. Phys. **123**, 055102 (2018).
[44] S. V. Razorenov, E. B. Zaretsky, and A. S. Savinykh, J. Phys. Conf. Ser. **500**, 112053 (2014).
[45] L. Wayne, K. Krishnan, S. DiGiacomo, N. Kovvali, P. Peralta, S. N. Luo, S. Greenfield, D. Byler, D. Paisley, and K. J. McClellan, Scr. Mater. **63**, 1065 (2010).
[46] B. Pang, S. Case, I. P. Jones, J. C. F. Millett, G. Whiteman, Y. L. Chiu, and C. A. Bronkhorst, Acta Mater. **148**, 482 (2018).
[47] B. W. Reed, J. S. Stolken, R. W. Minich, and M. Kumar, J. Appl. Phys. **110**, 113505 (2011).
[48] See Supplemental Material at http://link.aps.org/supplemental/10.1103/PhysRevLett.126.085503 for more discussions about simulation methods and theoretical models, which includes Refs. [49–55].
[49] J. P. Hirth, H. M. Zbib, and J. Lothe, Model. Simul. Mater. Sci. Eng. **6**, 165 1998.
[50] A. E. Mayer, K. V. Khishchenko, P. R. Levashov, and P. N. Mayer, J. Appl. Phys. **113**, 193508, 2013.
[51] Y. P. Varshi, Phys. Rev. B **2**, 3952 (1970).
[52] A. Yu Kuksin and A. V. Yanilkin, Phys. Solid State **55**, 1010, 2013.
[53] D. A. Matuska, HULL users' manual, AFATL-TR-84-59, National Technical Information Service, Springfield, VA, 1984.
[54] M. B. Bever, D. L. Holt, and A. L. Titchener, Prog. Mater. Sci. **17**, 5 (1973).
[55] H. Reismann and P. S. Pawlik, *Elasticity Theory and Application* (John Wiley, New York, 1980).
[56] S. Yao, X. Pei, Z. Liu, J. Yu, Y. Yu, and Q. Wu, Mech. Mater. **140**, 103211 (2020).
[57] C. Kittel, *Introduction to Solid State Physics* (Wiley, New York, 2004).
[58] M. A. Shehadeh, H. M. Zbib, and T. Rubia, Int. J. Plast. **21**, 2369 (2005).
[59] B. Devincre, T. Hoc, and L. Kubin, Science **320**, 1745 (2008).
[60] Z. Wang, O. Beyerlein, and R. LeSar, Model. Simul. Mater. Sci. Eng. **15**, 675 (2007).
[61] D. L. Preston, D. L. Tonks, and D. C. Wallace, J. Appl. Phys. **93**, 211 (2003).
[62] Y. Fan, Y. N. Osetsky, S. Yip, and B. Yildiz, Phys. Rev. Lett. **109**, 135503 (2012).
[63] B. Gurrutxaga-Lerma, M. A. Shehadeh, D. S. Balint, D. Dini, L. Chen, and D. E. Eakins, Int. J. Plast. **96**, 135 (2017).
[64] D. E. Grady, J. Geophys. Res. **85**, 913 (1980).